

Article

Flexural Performances of Novel Wet Joints with Sleeve Connections in Precast Composite Floor System

Wenbin Zhang ^{1,2}, Yan Feng ³, Xiangqiang Zeng ⁴, Ming Xu ^{3,*}, Liang Gong ^{1,2,*} and Lijun Rui ^{1,2}¹ Nanjing Vocational Institute of Transport Technology, Nanjing 211188, China² Technology Research Center for Green Building Engineering, Nanjing 211188, China³ Key Laboratory of RC&PC Structures of Ministry of Education, Southeast University, Nanjing 210096, China⁴ Shandong Shijia Yuanda Technology Development Co., Ltd., Qingdao 224000, China

* Correspondence: xuming@seu.edu.cn (M.X.); 230218129@seu.edu.cn (L.G.)

Abstract: A new type of assembled integral multi-ribbed composite floor system with novel wet joint and steel sleeve connections, which exhibits satisfactory strength and stiffness, was proposed in the previous study. To further study the flexural performances of the joints, six groups of specimens, including two cast in situ concrete slabs and four composite slabs sized 4700 mm × 1200 mm × 300 mm and 2450 mm × 1200 mm × 300 mm, were investigated under four-point flexural tests. Four main influence factors were experimentally studied, i.e., casting methods, joint amounts, shear span lengths, and steel sleeve layout directions, on the failure modes, crack distributions, and deflection-load carrying capacity relationship. Test results indicated that the proposed composite slab system could provide the ultimate bearing capacity lower by 7% than that of the cast in situ concrete slabs, largely exceeding the code-predicted strength. No strain difference between the steel sleeve connections and steel rebars indicated good wet joint connection behavior. More hollow-core sections and long shear spans increased the potential of interfacial splitting cracks, leading to a shorter elastic stage and lower elastic stiffness. A finite element model was further parametrically conducted to explore the structural performances. Finite element results also indicate that the precast concrete slab had a more significant influence on the failure loads than the influences of concrete compressive strength and lap-splice steel rebar strength. These findings indicate that the proposed composite slab systems possess a satisfactory performance in the ultimate bearing capacity and deformability. Thus, such an assembled integral multi-ribbed composite floor system can be widely applied in construction.

Keywords: assembled integral structure; composite slabs; precast slabs; steel sleeve connections; flexural performances



Citation: Zhang, W.; Feng, Y.; Zeng, X.; Xu, M.; Gong, L.; Rui, L. Flexural Performances of Novel Wet Joints with Sleeve Connections in Precast Composite Floor System. *Buildings* **2024**, *14*, 822. <https://doi.org/10.3390/buildings14030822>

Academic Editor: Dan Bompa

Received: 12 January 2024

Revised: 26 February 2024

Accepted: 1 March 2024

Published: 18 March 2024



Copyright: © 2024 by the authors. Licensee MDPI, Basel, Switzerland. This article is an open access article distributed under the terms and conditions of the Creative Commons Attribution (CC BY) license (<https://creativecommons.org/licenses/by/4.0/>).

1. Introduction

Floor systems are horizontal load-bearing components in buildings that carry and transmit gravity and live loads to the vertical load-bearing members. Especially when an earthquake occurs, the floor system could effectively distribute the seismic force in the entire building through the lateral force members [1]. So far, three types of floor structures have been widely used: cast in situ floor, precast floor with cast in situ concrete topping, and untopped precast floor. As a labor-saving, environment-friendly, and low-carbon construction method, the precast concrete (PC) technology shows great potential in promoting construction efficiency and improving product quality since such a composite floor system reduces the amount of formwork, wet work, and construction pollution compared to casting in situ [2–7]. Thus, precast composite floor systems have always been of interest and widely used in buildings to fully combine the advantages of both cast in situ construction and prefabricated elements [8–12].

Currently, studies on the development and performance of precast composite systems have been conducted and evaluated comprehensively. Test results [9,10,13] indicated that

cast in situ concrete toppings enabled an enhancement of the shear capacity of the precast concrete slab when the interfacial bond strength was ensured. Additionally, the use of autoclaved aerated concrete blocks filling into the precast concrete slab was demonstrated to remarkably reduce the self-weight under the same flexural capacity requirements [14,15]. A new type of discrete connected precast reinforced concrete diaphragm floor system, comprising the precast flat slabs and slab joint connectors [16], was proposed. Test results indicated that the load-bearing capacity and stiffness of such a composite system increased considerably as the hairpin and cover plate hybrid slab joint connectors effectively ensured their cooperation in transmitting the shear and moment force. In addition, the self-weight of the floor system accounted for over 40% of the entire structural mass. A reduced self-weight of the composite slab would decrease the dead load, contributing to a lower seismic response of the structure, thereby reducing the lower requirement for the bearing capacities of the beam, column, and shear wall [17,18]. The lightweight composite slab had an additional advantage in facilitating the hoist and installation during its construction. Therefore, precast hollow-core and double tee slabs were commonly used [2].

In addition, the joint configurations in the precast concrete slab system played a crucial role in improving the performance of composite floors. It is demonstrated that a lap-spliced rebar placed on the top of precast concrete units could provide comparable flexural performance to cast-in-place concrete slabs [19]. A novel precast concrete slab with crossed bent-up rebar was proposed and tested on its flexural mechanism by Chen et al. [20]. It was found that the horizontal component force of the bent-up ends increased the flexural strength of the joint, whereas the vertical component force of the bent-up ends enhanced the anchorage performance between the precast units and top-covering concrete. To improve the ease of construction of large-span floors, Huang et al. [21] developed an assembly integral floor structure voided with steel mesh boxes. Experimental results supported that the design had a high bi-directional vertical bearing capacity. Additionally, a test on lightweight engineering cementitious composite-normal concrete precast slabs with lattice girders by Deng et al. [22] confirmed that such a composite system reduced its self-weight and improved the flexural performance. Similarly, the flexural behavior of steel-concrete ultra-shallow floor beams with precast hollow-core slabs was established and studied to overcome the shortcomings of the need for heavier steel profiles, maximizing costs, and higher floor sections with the increase in span. Increasing the thickness of the concrete topping increased the resistance and stiffness of the composite section, whereas the reinforcement ratio showed a slight influence on the resistance.

To reduce the self-weight of the floor system and improve the construction efficiency, a new type of assembled integral two-way multi-ribbed composite floor system was proposed by Zeng et al. [23]. It is shown in Figures 1 and 2 and comprised four main parts: precast multi-ribbed bottom slab (PRBS), lightweight infills, cast in situ upper slab (CUS), and joints. Using the PRBS and a lightweight infill cavity could lead to a high hollow ratio of 43% and an assemble ratio of 87%, respectively, showing a tremendous economic benefit. The force transfer between the PRBS and CUS was realized by the interfacial friction, stirrups, and cast in situ joints. Lightweight infills were used to form the hollow core of the whole floor slab and increase the capability of maintaining the room temperature and sound absorption, which were fixed on the precast bottom slab through the positioning rebars. Steel sleeves connected the lap-splice rebars in the joint to facilitate the construction and ensure connection behavior. In reference [23], a full-scale static experiment has been carried out, revealing that the anti-crack property, elastic stiffness, and load-carrying capacity are all greater than the Chinese design codes and have enough safety redundancy.

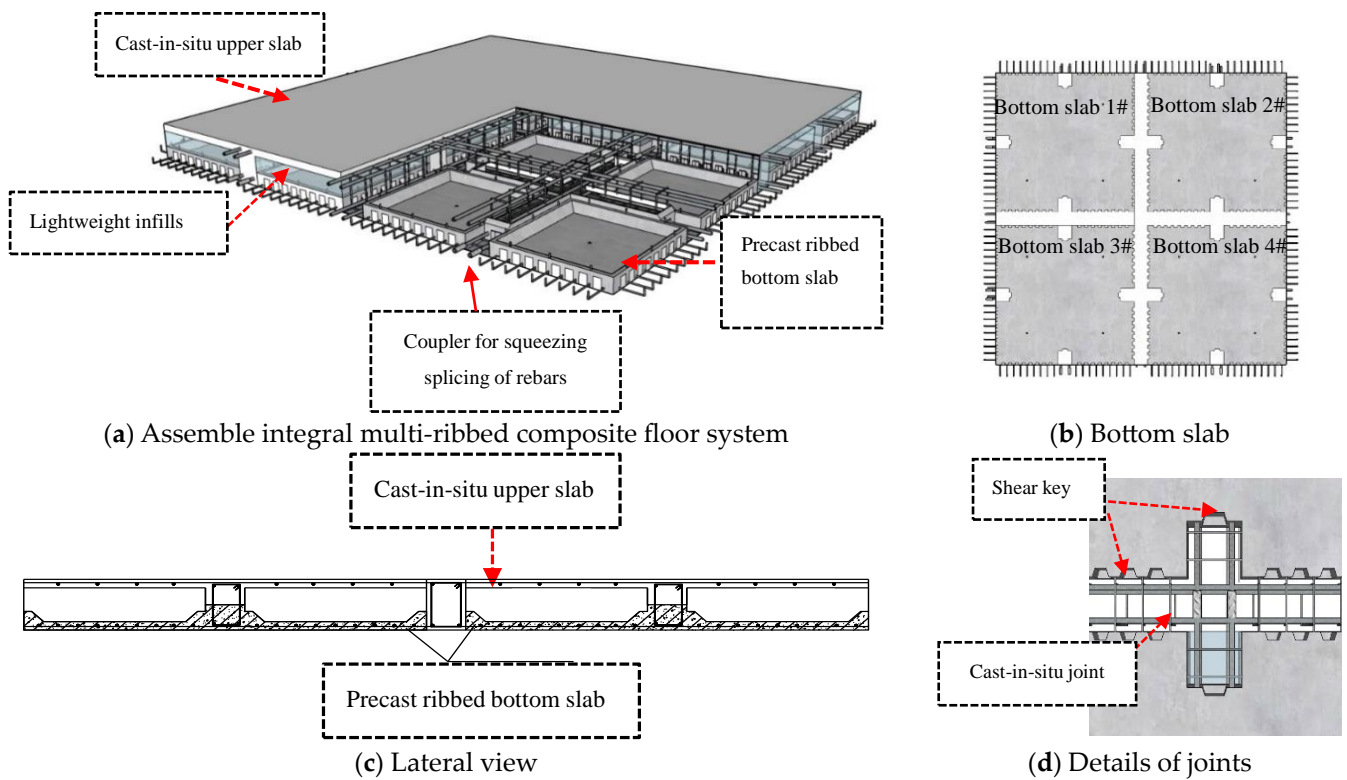


Figure 1. Schematic of the assembled integral multi-ribbed composite floor system.

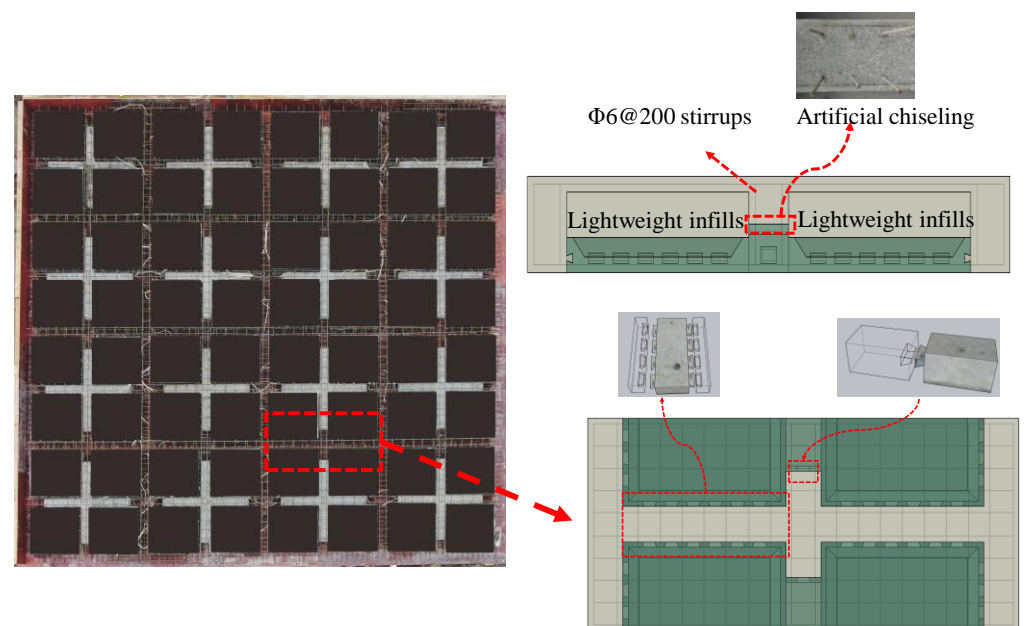


Figure 2. Typical wet joint of the assembled integral multi-ribbed composite floor system.

The mechanical performance of the joint is the key to the assembled integral structures according to research around the world. The assembled integral two-way multi-ribbed composite floor system with steel sleeve connections has been validated to have superior anti-crack strength, elastic stiffness, and load-carrying capacity using full-scale tests [23]. However, such a structure's performance, including the steel sleeve connection, has not been understood clearly in the one-way multi-ribbed composite floor system, which has delayed its wide engineering application. In order to close the gap, six specimens were tested to consider the influences of span lengths, concrete casting methods, and steel

sleeve directions on the failure loads, crack distribution, and load-midspan deflection. The prediction of the ultimate bearing capacity was also compared with the current design codes, and numerical analysis was further conducted to explore the structural performances.

2. Experimental Program

2.1. Specimen Details and Material Properties

As aforementioned, a full-scale specimen of the proposed assembled integral multi-ribbed composite floor system sized 9600 mm × 9600 mm has been tested under uniform area load. The typical forms of the composite joint could be easily identified from the designed files, as presented in Figure 2. Roughly concluded, the wet joints could be categorized into four types, which are 2450 mm specimens with one or two joints and 4700 mm specimens with one or two joints.

Six precast composite slabs with steel sleeve connections were fabricated to study the mechanical performance of one-way precast composite slabs with sleeve connections. All specimens had the same width of 1200 mm and height of 300 mm. The investigated parameters are listed as follows: two beam lengths (2450 and 4700 mm), the casting type of slabs (cast in situ and precast composite slab), the sleeve layout directions (longitudinal and transverse direction), the number of wet joints (0, 1 and 2), and shear span length (500 and 1225 mm). The dimensions and details of the specimen are shown in Figure 3a–d and Table 1. Table 1 lists the specimen ID by the casting method, loading type, joint amount, beam length, and sleeve directions. For example, the specimen CB-F-0-24-0 refers to the cast in situ concrete slab of 2450 mm span length without joints and sleeves under a flexural loading test, whereas specimen PB-FS-2-47-L denotes the precast composite slabs of 4700 mm span length with two joints and longitudinal sleeves under flexural-shear loading. The longitudinal and transverse directions refer to the beam span and cross-sectional directions. Specimens CB-F-0-24-0 and CB-FS-0-47-0 were used as the control beams. Each group had two repeated samples. Note that the specimens CB-F-0-24-0 and CB-FS-0-47-0 had the same configuration as specimens PB-F-1-24-L and PB-FS-2-47-L, except for the joints and sleeves due to the cast in situ method used.

The steel reinforcements of 8, 16, and 20 mm diameter had an average yielding strength of 436.4, 451.2, and 420.3 MPa, respectively, whereas their ultimate strengths were tested for 580.5, 616.6, and 620.1 MPa. Accordingly, the elastic modulus was tested for 213.5, 209.6, and 217.7 GPa. The 16 mm diameter sleeves had yield and ultimate strengths of 450 and 604 MPa, while the 20 mm diameter sleeves were tested for 431 and 610 MPa, respectively.

The cubic compressive strength and elastic modulus of concrete were 39.5 MPa and 29.6 Gpa, respectively.

Table 1. Details of the tested specimens.

Specimen ID	Joint Amount	Dimension/mm	Sleeve Direction	Loading Type	Casting Method	Duplicate	S_d /mm
CB-F-0-24-0	0	2450	-	F	Cast in situ	2	1250
CB-FS-0-47-0	0	4700	-	FS	Cast in situ	2	2050
PB-F-1-24-T	1	2450	Transverse	F	Precast	2	1250
PB-F-1-24-L	1	2450	Longitudinal	F	Precast	2	1250
PB-FS-2-47-L	2	4700	Longitudinal	FS	Precast	2	2050
PB-FS-2-47-T	2	4700	Transverse	FS	Precast	2	2050

Note: F refers to the specimen in flexure, FS indicates the specimen in flexural shear, and S_d refers to the distance between two loading points.

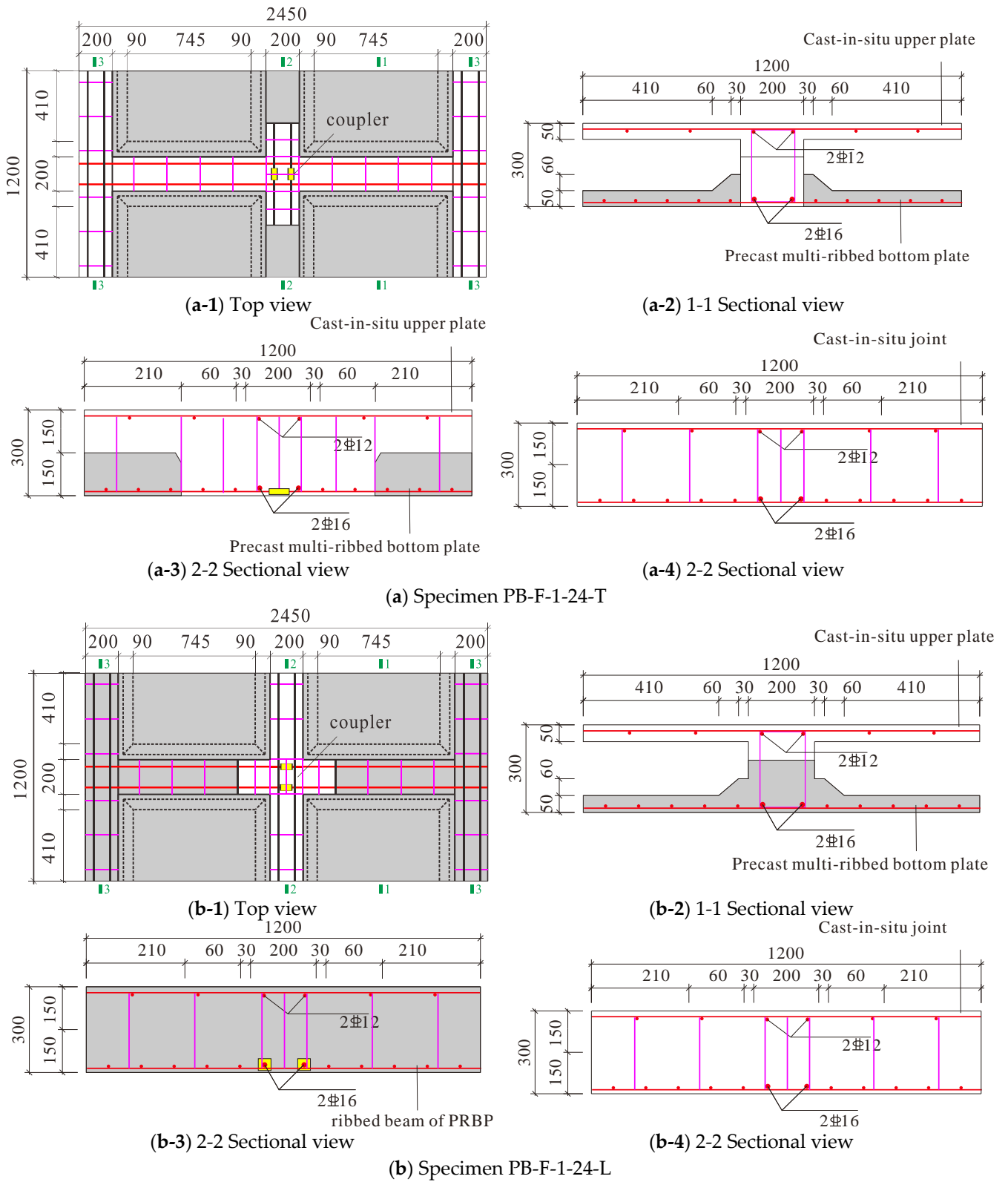


Figure 3. Cont.

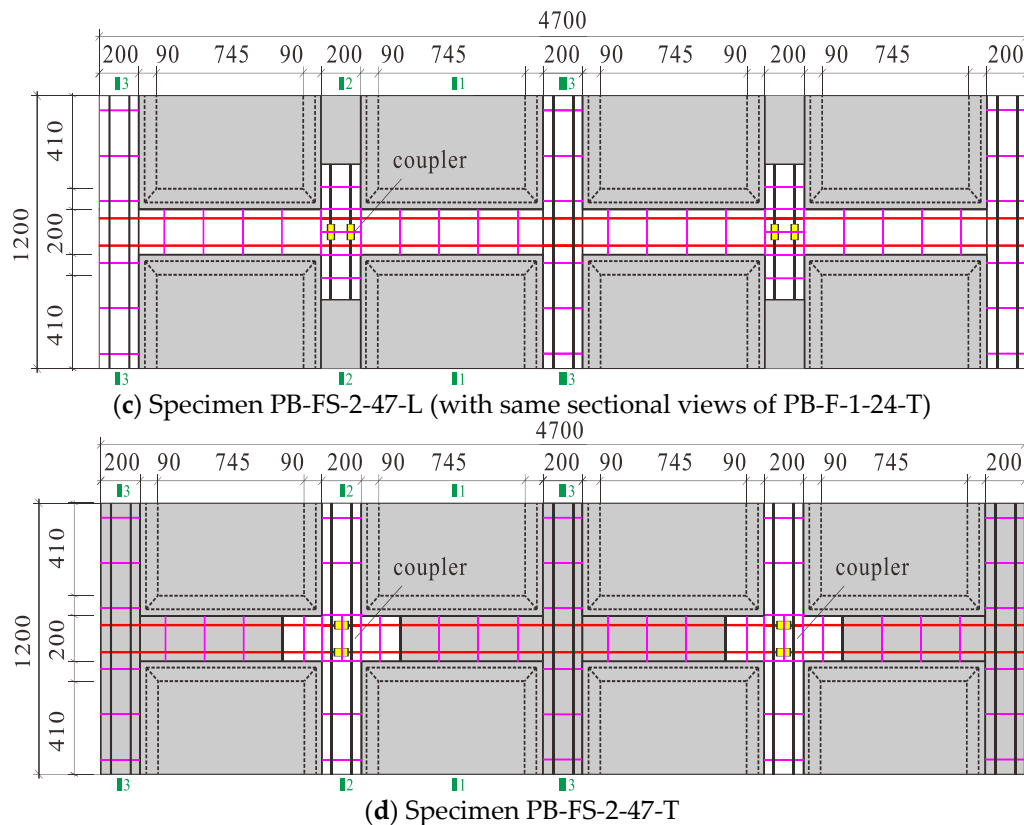


Figure 3. Details of the tested specimens (with the same sectional views as PB-F-1-24-L).

2.2. Test Setup and Measuring System

Figure 4a,b shows a schematic diagram of the test loading setup. All specimens were placed horizontally on a fixed hinge device at the left end and a sliding hinge device at the right end. As presented in Table 1, the distances between the two loading points are 1250 and 2050 mm, respectively, for the specimens with 2450 and 4700 mm length. Two spreading steel plates were placed along the slab width direction at two loading points to transfer the loads from the hydraulic jack to the specimen. The loading process was conducted following the Chinese standard for test methods of concrete structures [24], in which, when the major crack width achieved above 1.5 mm or the mid-span deflection exceeded 1/50 of the span length, the loading was ended. Before the formal loading of the specimen, the pre-loading to 10 kN and then unloading to 0 kN was conducted to ensure the function of the measure and loading system. When the specimen was formally loaded, an increment of 15 kN was applied to the specimen until the midspan deflection of 20 mm, after which the load increment was reduced to 5 kN and maintained for 5 min to observe the stable values of the strain gauges and deflections, ensuring the safety of the experimental person.

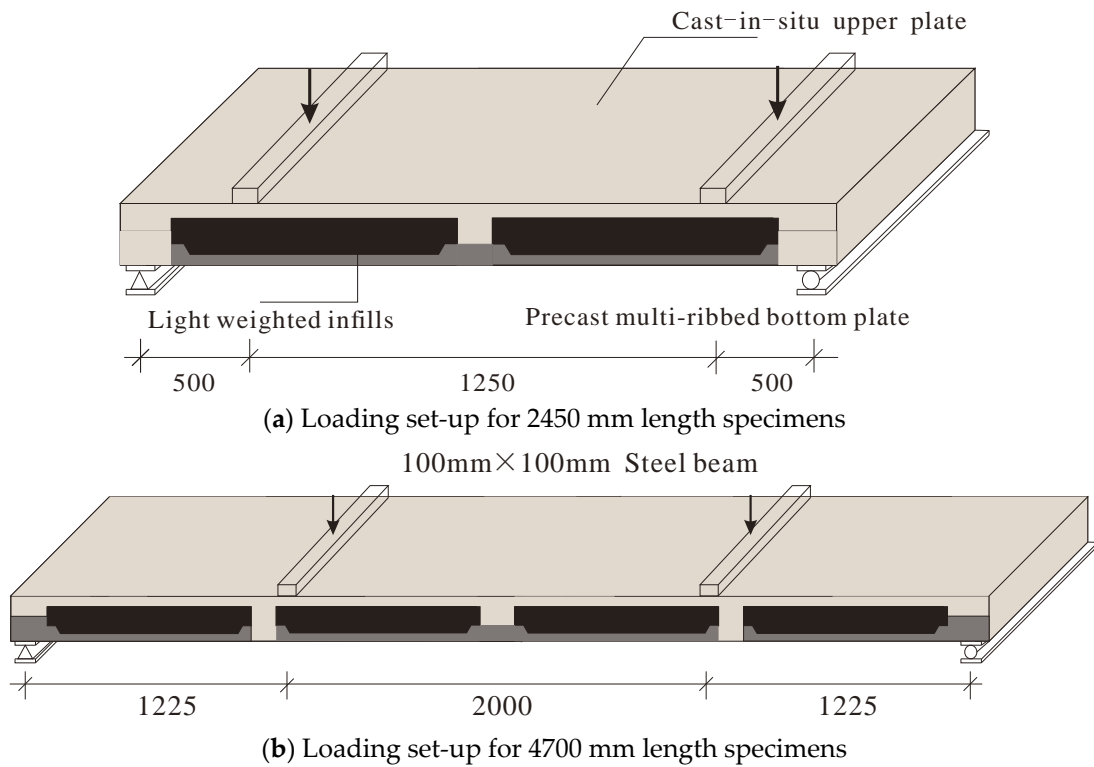
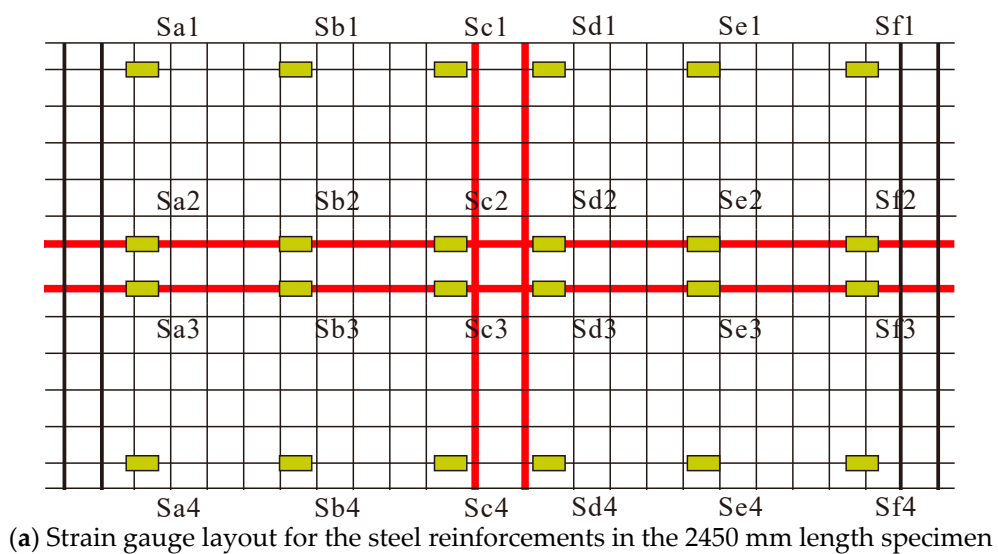


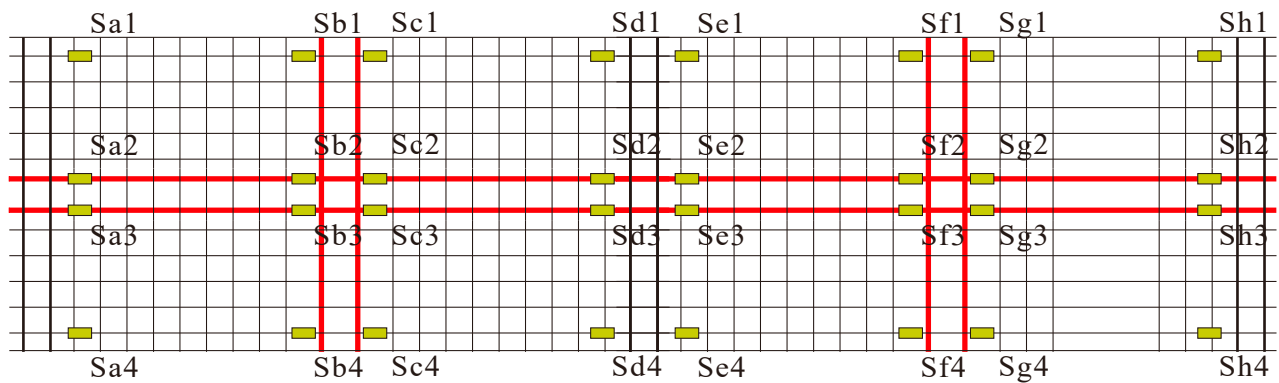
Figure 4. Test setup for the specimens.

To distinguish the differences in the loading transfers and crack propagations between the cast in situ slab and composite slabs, the strain gauges for the concrete and steel reinforcements were employed to observe the strain evolutions, especially for the steel reinforcements and the concrete in the joints. Figure 5a,b shows the strain gauge layout for the steel reinforcements in the 2450 and 4700 mm length specimens, respectively. In addition, to observe the structural behavior of the 2450 mm length slabs, four Linear Variable Displacement Transducers (LVDTs) were placed at two supports, and one LVDT was used to detect the midspan deflection (also at the joint), as shown in Figure 5c. In contrast, for the 4700 mm length specimens, two LVDTs were put at two supports, whereas three LVDTs were located at each joint within the midspan, as presented in Figure 5d.

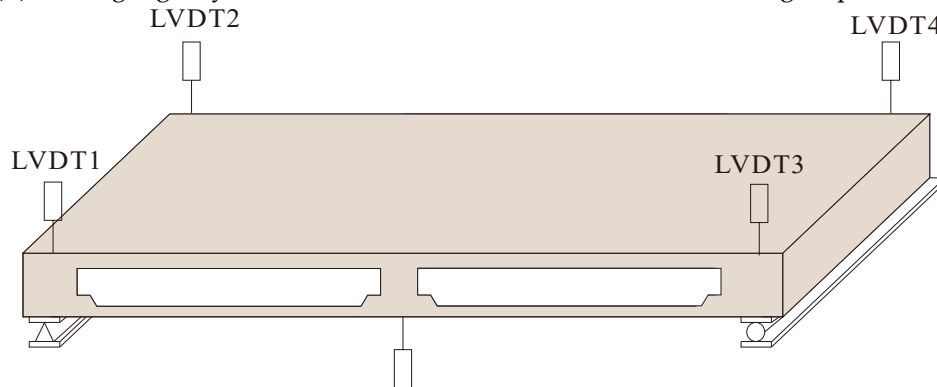


(a) Strain gauge layout for the steel reinforcements in the 2450 mm length specimen

Figure 5. Cont.



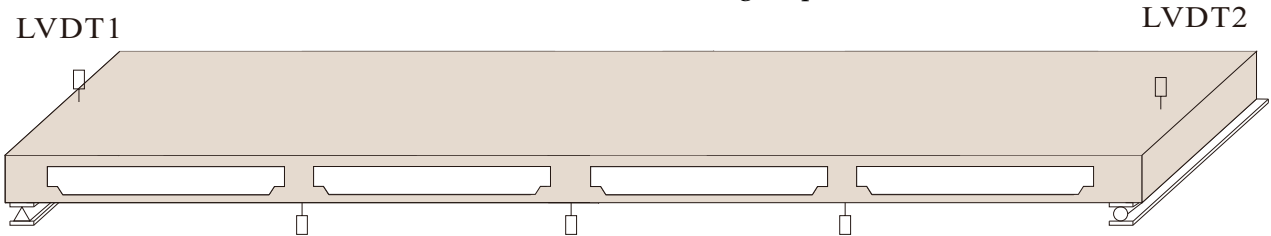
(b) Strain gauge layout for the steel reinforcements in 4700 mm length specimens



LVDT5、6、7

(arranged at the middle and two sides, respectively)

(c) LVDT for the 2450 mm length specimen

LVDT3 LVDT5、6、7 LVDT4
(arranged in the middle and two sides, respectively)

(d) LVDT layout for the 4700 mm length specimen

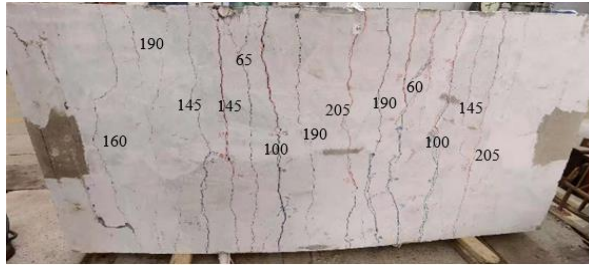
Figure 5. Schematic diagram of the measuring points for the tested specimens.

3. Results and Discussion

3.1. Failure Modes and Crack Patterns

Figure 6a–l shows the failure modes, and Figure 7a–l presents the schematic diagram of crack patterns of all tested specimens. For the cast in situ 2450 mm length specimens, the flexural-shear failure occurred for specimen CB-F-0-24-0 (Figure 6a,b), with the flexural cracks on the bottom (Figure 6(a-1,b-1,e-1,f-1,g-1,h-1,i-1,j-1,k-1,l-1)), top (Figure 6(a-2,b-2,e-2,f-2,g-2,h-2,i-2,j-2,k-2,l-2)) and lateral surface (Figure 6(c,d,e-3,f-3,g-3,h-3,i-3,j-3,k-3,l-3)) of the concrete slab and diagonal cracks occurring on the shear span of the slabs. At failure, the concrete within the flexural-shear span was crushed; the major crack width achieved was up to 10 mm, and the tensile strain in the longitudinal steel reinforcements yielded up to 2000 $\mu\epsilon$. In contrast, specimen CB-F-0-47-0 (see Figure 7c,d) cracked earlier than specimen CB-F-0-24-0 (see Figure 7a,b) at the loading and constant moment regions. With the increasing load, the transverse cracks along the slab direction gradually occurred at the

intersection of the rib and web of the beam and penetrated through the whole cross-section. When the diagonal cracks appeared, a rapid increase in the deflection was observed. The specimen's deflection (up to 80 mm) and maximum crack width (up to 15 mm) were too large to bear further loads. Therefore, no pronounced crushing failure occurred, as presented in specimen CB-F-0-24-0, indicating that the governed failure was determined by the structural deformability rather than the ultimate bearing capacity.



(a-1) Bottom surface



(a-2) Top surface

(a) Specimen CB-F-0-24-0-1



(b-1) Bottom surface



(b-2) Top surface

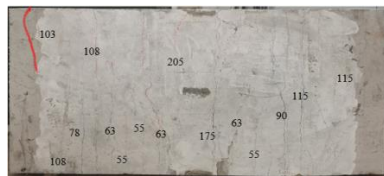
(b) Specimen CB-F-0-24-0-2



(c) Specimen CB-F-0-47-0-1



(d) Specimen CB-F-0-47-0-2



(e-1) Bottom surface



(e-2) Top surface

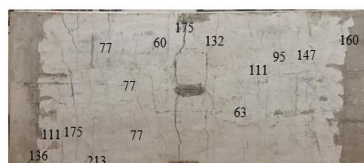
(e) Specimen PB-F-1-24-T-1



(e-3) Cracks at the joint



(f-1) Bottom surface



(f-2) Top surface

(f) Specimen PB-F-1-24-T-2



(f-3) Cracks at the joint

Figure 6. Cont.

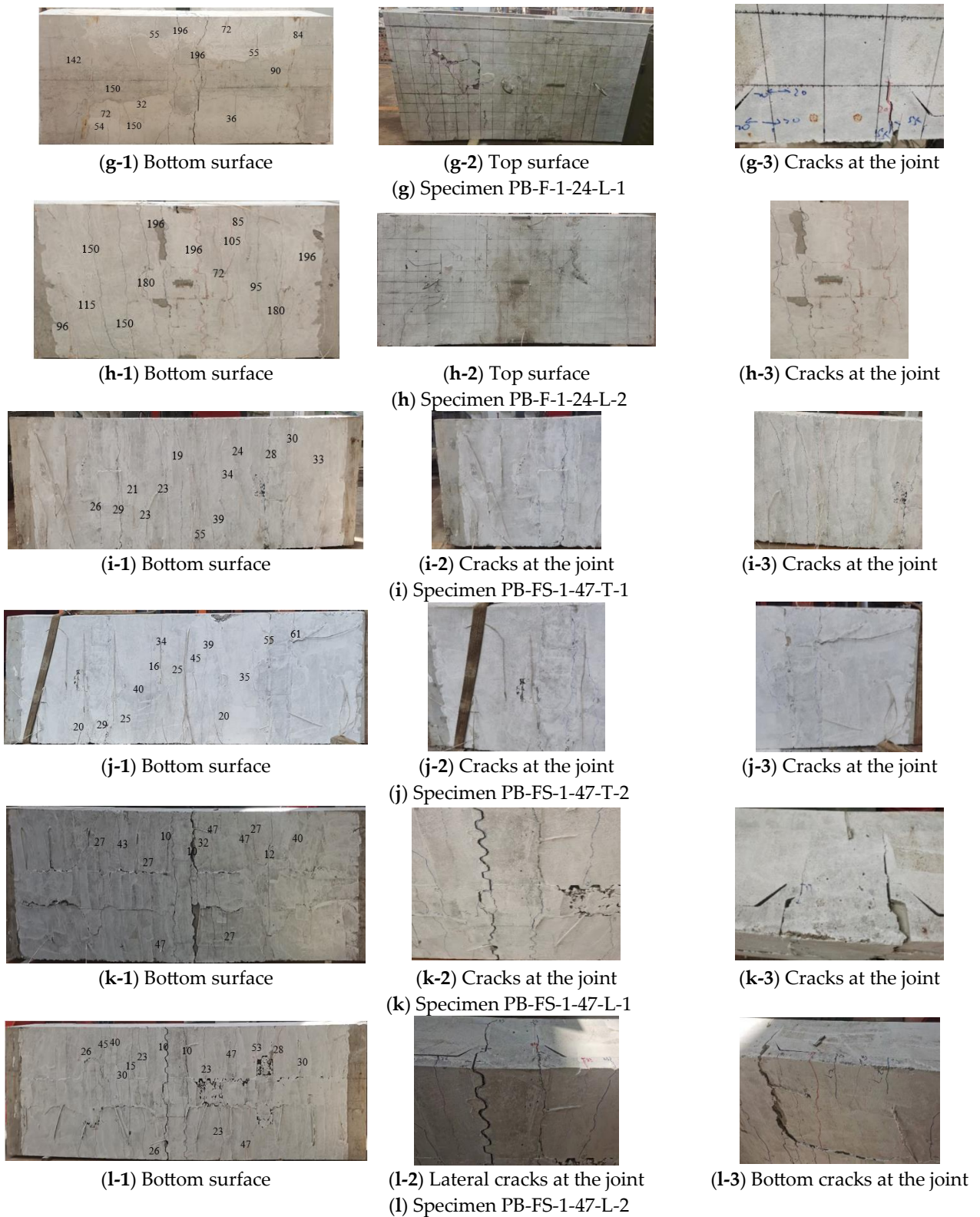


Figure 6. Failure modes of all tested specimens.

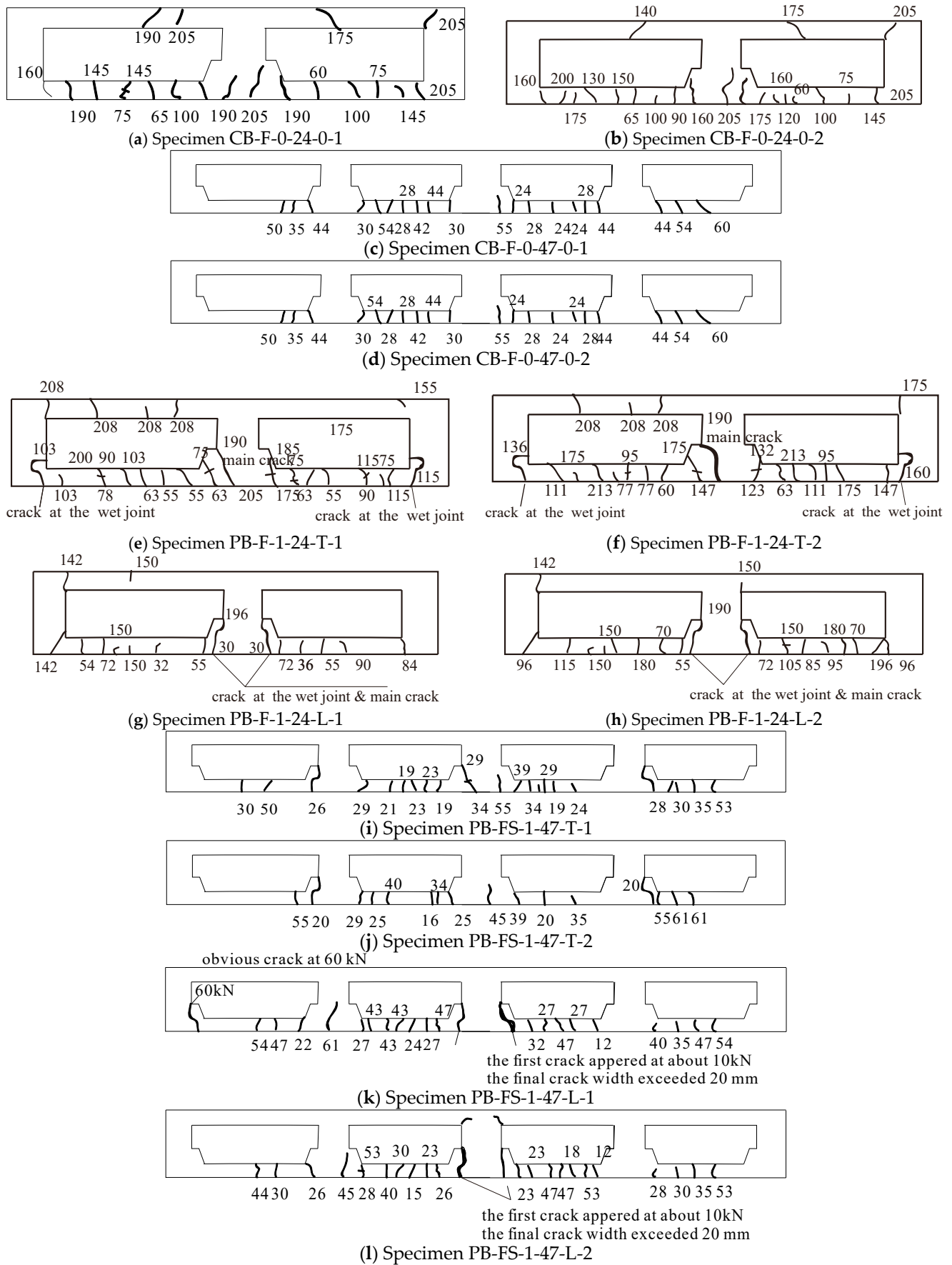


Figure 7. Schematic diagram of crack distributions of all tested specimens.

For specimen PB-F-1-24-T, with precast concrete layers and transversely installed sleeves (see Figure 7e,f), transverse cracks along the slab width direction gradually initiated at the hollow-core section within the constant moment region and propagated through the whole cross-section. As the load increased to 105 kN, visible cracks initiated at the interface between the cast and precast concrete. Compared to the cracks developed earlier, the interfacial cracks did not propagate along the whole slab width but toward the ribbed slabs. When the longitudinal steel reinforcements yielded, numerous diagonal cracks formed near the wet joints on the lateral surface of the slab. The maximum crack width increased up to 10 mm, eventually resulting in the shear failure of the composite slab. However, when the sleeves were installed along the longitudinal direction, as shown in specimen PB-F-1-24-L (see Figure 7g,h), the concrete near the loading point at the bottom surface of the slab cracked earlier. Then, the flexural cracks continuously formed and opened with an increasing deflection. At a load of 190 kN, shear failure of the inner embedded cavity occurred, indicating the control of failure by the weakened wet joint.

When the beam span length increased to 4750 mm for specimen PB-FS-2-47-L (see Figure 7k,l), the concrete cracks initiated from the bottom surface within the constant moment region and passed through the entire cross-section rapidly. The joints within two loading points then cracked and propagated across the slab's width, and the cross-section at the intersection between the precast ribbed slab and cast in situ concrete layer began to crack until 45 kN. Afterward, no new cracks occurred in the constant moment region while new diagonal cracks developed and accumulated. The loading process ended with the maximum crack width reaching its limit. In contrast, the elastic stage was shorter when the sleeves were installed along the slab width direction in specimen PB-FS-2-47-T (see Figure 7i,j). The crack first occurred at the joint interface between the precast ribbed beam and the cast in situ concrete layer. The flexural cracks on the bottom surface of the slab continuously developed while the previous crack at the joint just gradually opened. As the load increased to 40 kN, the crack occurred at the abruptly changed cross-section and rapidly crossed through the entire section. Afterward, no new crack appeared within the constant moment region but occurred at the shear span. The specimen could not bear further loads with increasing deflections and maximum crack width.

3.2. Moment–Midspan Deflection Relationships

Figure 8 presents the moment–midspan deflection curves of all tested specimens. It is observed that all curves show three typical stages, including the elastic stage, the concrete cracking until the yielding of steel reinforcements, and the post-yielding stage. Compared with the cast in situ specimens CB-F-0-24-0 and CB-F-0-47-0 (see Figure 8a,b), the precast composite slab had a comparable ultimate moment within a decrease by 7%, except for a 13% decrease in specimen PB-F-1-24-L (see Figure 8c,d). It indicates that such a precast composite slab system using the sleeve connections had a good ultimate bearing capacity. However, note that the sleeve along the longitudinal direction of the slab more significantly reduced the composite slabs' ultimate strength relative to that of transversely placed sleeves. The longitudinal sleeves negatively affected the continuous load transfer of the normal stress induced by the moment. The joint between the precast slab and cast in situ concrete was easier to crack, and more cracks developed near the joint, preventing the load from being transferred to the uncracked parts. In addition, the joint crack caused interfacial slip between the precast slab and the cast in situ concrete layer. It resulted in an additional midspan deflection and wider cracks, leading to failure at a smaller ultimate load. Also, the ductility, defined as the ratio of yielding deflection to the ultimate deflection, was decreased by 40% and 34%, respectively, compared to the cast in situ specimens of 2450 mm length, whereas 42% and 27% decreases were observed for the specimens of 4700 mm length. The smaller reduction indicated that failure caused by a larger shear span-to-depth ratio (in specimen with 4700 mm length, see Figure 8e,f) had better flexural deformability. More shear keys in the longer shear span resulted in a smaller shear slip, resulting in fewer splitting interfacial cracks but more flexural cracks, as validated in Figure 7, which

increased the ductility. Therefore, the precast composite slab had a lower post-yielding deformability than the cast in situ slabs.

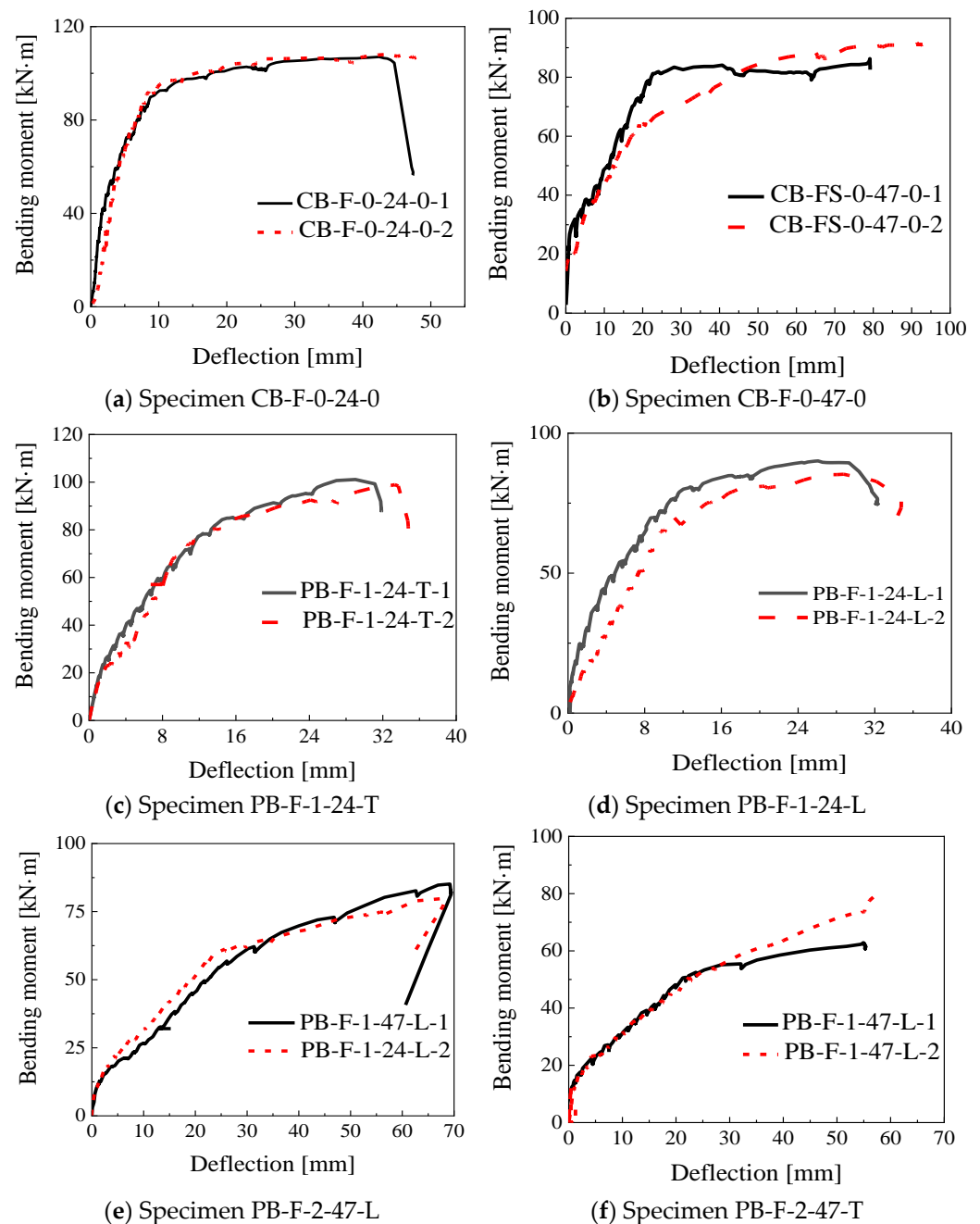


Figure 8. Moment–midspan deflection relationship.

3.3. Strains in the Sleeves and Steel Reinforcements

Figure 9 shows the strain evolution in the sleeves and steel reinforcements, the labels of which are marked in Figure 5. The red and blue lines refer to the yielding strains of steel reinforcements and steel sleeves, respectively, which were tested for 2000 and 2400 $\mu\epsilon$. This figure shows no noticeable strain difference between steel reinforcements and connected sleeves. The sleeves achieved 2000 $\mu\epsilon$, corresponding to the yielding strain of steel reinforcements. The maximum strains for specimens CB-F-0-24-0, PB-F-1-24-T, and PB-F-1-24-L were measured for 3000 $\mu\epsilon$, 2500 $\mu\epsilon$, and 4000 $\mu\epsilon$, which were tested for 3000 $\mu\epsilon$, 6000 $\mu\epsilon$, and 6000 $\mu\epsilon$ for specimens CB-F-0-47-0, PB-F-2-47-L, and PB-F-2-47-T. The larger strain values obtained in the latter specimen indicated that the steel reinforcements

with sleeves could still ensure the connection strength and deformability, showing a reliable connection construction, particularly for large deflections in the longer-span slabs.

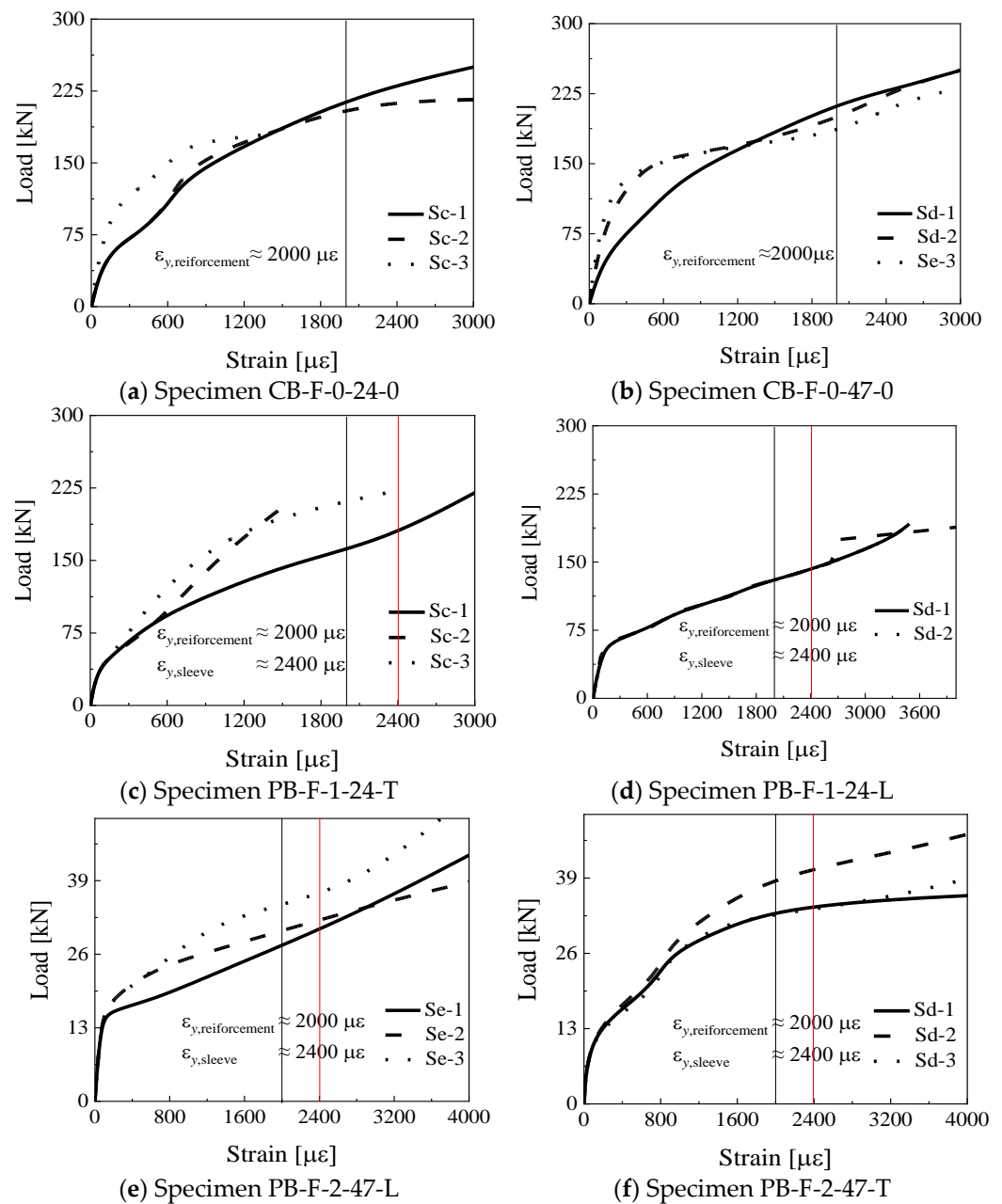


Figure 9. Strain in the sleeves and steel reinforcements.

4. Evaluation of Ultimate Bearing Capacity

The ultimate bearing capacity of the tested specimens was predicted based on the Chinese design codes [24], in which the effective compressive flange width was determined, and the self-weight of the slabs was not considered. Two 16 mm diameter steel reinforcements were used to carry the longitudinal tensile stress, while the 6 mm diameter steel reinforcements were provided as the constructional reinforcements. The hollow-core composite slab was regarded as a wide flange I-shaped section. The flange width in the compressive zone was calculated using Equation (1). Then, the flexural strength of the composite slab can be calculated as a rectangular cross-section, shown as the following Equations (2) and (3):

$$b = b_0 + 12h'_f \quad (1)$$

$$M = \alpha_1 f_c b x (h_0 - x/2) + f_y' A_s' (h_0 - \alpha_s') \quad (2)$$

$$\alpha_1 f_c b x = f_y A_s - f_y' A_s' \quad (3)$$

where b_0 is the width of the ribbed beam, h_f is the flange depth, α_1 is the coefficient, which is set as 1.0 for a compressive strength smaller than 50 MPa, f_c is the compressive strength of the concrete, A_s and A_s' are the area of the steel reinforcements in the tensile and compressive zones, respectively, h_0 is the effective slab depth, f_y and f_y' are the yielding strengths of the tensile and compressive steel reinforcements, respectively, α_s' is the resultant compressive force from the steel reinforcements in the compressive zone.

Table 2 lists the comparisons between the test and theoretical values of all specimens. It is seen that the test-to-prediction results ratio was above 1.91, which largely exceeded the regulated value of 1.6 in the design code [25]. Thus, the proposed precast composite slab systems with ribbed slabs and sleeve connections could provide a reliable resistance satisfying the code requirements.

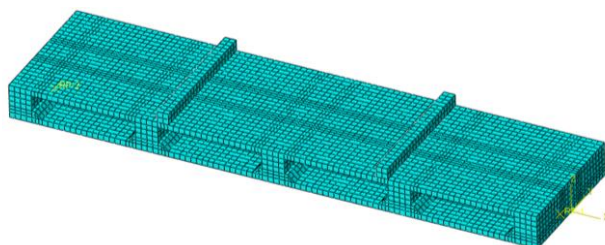
Table 2. Comparisons between test and calculation results.

Specimen ID	CB-F-0-24-0	CB-FS-0-47-0	PB-F-1-24-T	PB-F-1-24-L	PB-FS-2-47-L	PB-FS-2-47-T
Ultimate moment/ M_u	111.16	105.46	103.58	96.46	99.98	95.95
Predicted moment/ M_c	50.28	50.28	50.28	50.28	50.28	50.28
M_u/M_c	2.21	2.09	2.06	1.92	1.99	1.91

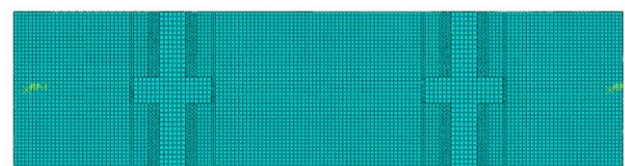
5. Finite Element Analysis of Assembly Integral Floor System

5.1. Finite Element Model

A refined finite element (FE) model was established using the commercial software ABAQUS 6.14 [26] for a more profound and parametric understanding of the mechanical properties of the assembly integral floor system with sleeve connections. This model (see Figure 10) used a three-dimensional eight-node element with reduced integral element (C3D8R) to simulate the PRBS, CUS, and sleeves. Three-dimensional two-node (T3D2) truss elements were applied to simulate the steel reinforcement behavior. The structured mesh method was used for all parts, and 8548, 15,096, 17,774, 13,951, 35,356, and 27,724 elements were obtained for specimens CB-F-0-24-0, CB-FS-0-47-0, PB-F-1-24-T, PB-F-1-24-L, PB-FS-2-47-L, and PB-FS-2-47-T, as in the reference of Figiel et al. [27]. The concrete damage plasticity model modeled the material properties of the concrete in the software. Parameters, i.e., the density, Poisson's ratio, dilation angle, eccentricity, biaxial-to-uniaxial compressive strength ratio of σ_{b0}/σ_{c0} , the influencing parameters of yielding surfaces K_c , and the viscosity parameter, were defined as 2450, 0.2, 30, 0.1, 1.16, 0.6667, and 0.005, respectively. The constitutive laws for steel reinforcements and concrete were adopted as defined in the Chinese design code [24].



(a) FE model of the composite slabs



(b) Mesh of specimen PB-F-1-24-T

Figure 10. FE model of the composite slabs.

All steel reinforcements were embedded in the concrete without considering the bond-slip behavior. The frictional constraint was used to simulate the connection behavior of

both shear keys and the sleeve connections, in which the normal direction was set as “hard contact” and the tangential direction was set as “penalty friction” with a coefficient of 0.4. The loading points, set as reference points, are coupled with the loading surfaces on the slabs. The boundary conditions for simply supported composite slabs were defined as a pinned support at the left and sliding support at the right. The general static solution method is adopted, and the load is applied by automatic increments with a minimum tolerance for convergence of 10^{-5} of externally applied loads.

5.2. FE Model Validation and Discussion

The influence of the span length of the composite slabs was not considered herein. The FE results for the 2450 mm length specimen were considered and validated with test results as stated earlier from both the crack pattern and load-midspan deflection curves. Figure 11 compares the crack pattern of specimens PB-F-1-24-T and PB-F-1-24-L, respectively. The maximum strain region in the contour confirmed the observed crack locations in the test for PB-F-1-24-T and PB-F-1-24-L. Figure 12 compares load-midspan deflection relationships of the tested cast in situ and precast composite slabs. It is seen that the FE-predicted curves agree well with the test curves, especially for the ultimate bearing capacity. However, note that the ultimate midspan deflection had a large error with the tested values. This was because the concrete in the tested slabs was not crushed as simulated in the FE model. The slip of sleeves and cracking behavior along the precast and cast in situ concrete interface might occur on approaching the failure, which leads to a large ultimate midspan deflection. Thus, the FE-predicted midspan deflection was relatively larger than the test values. Overall, the FE model could accurately predict the load-midspan deflection relationships.



Figure 11. Comparisons between the test and FE results for the crack evolution.

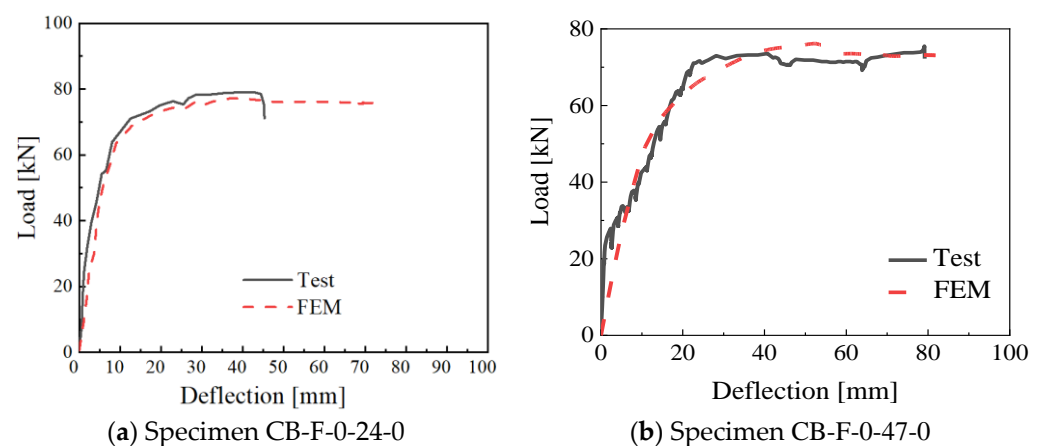


Figure 12. Cont.

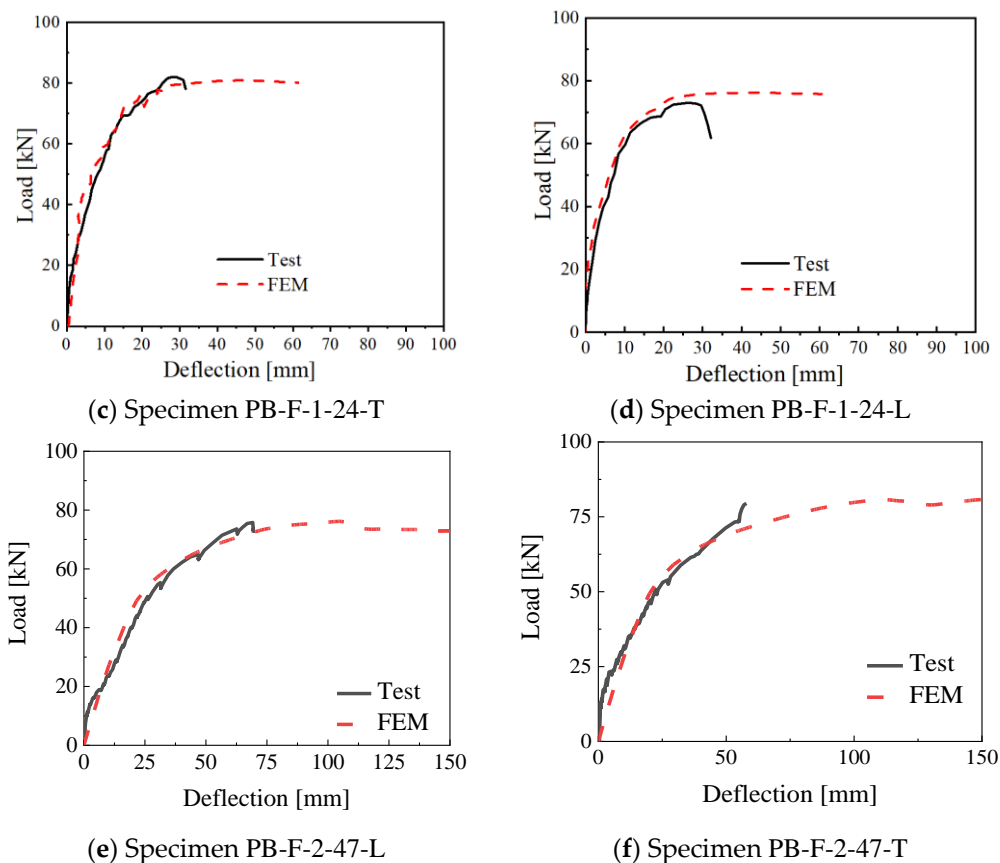


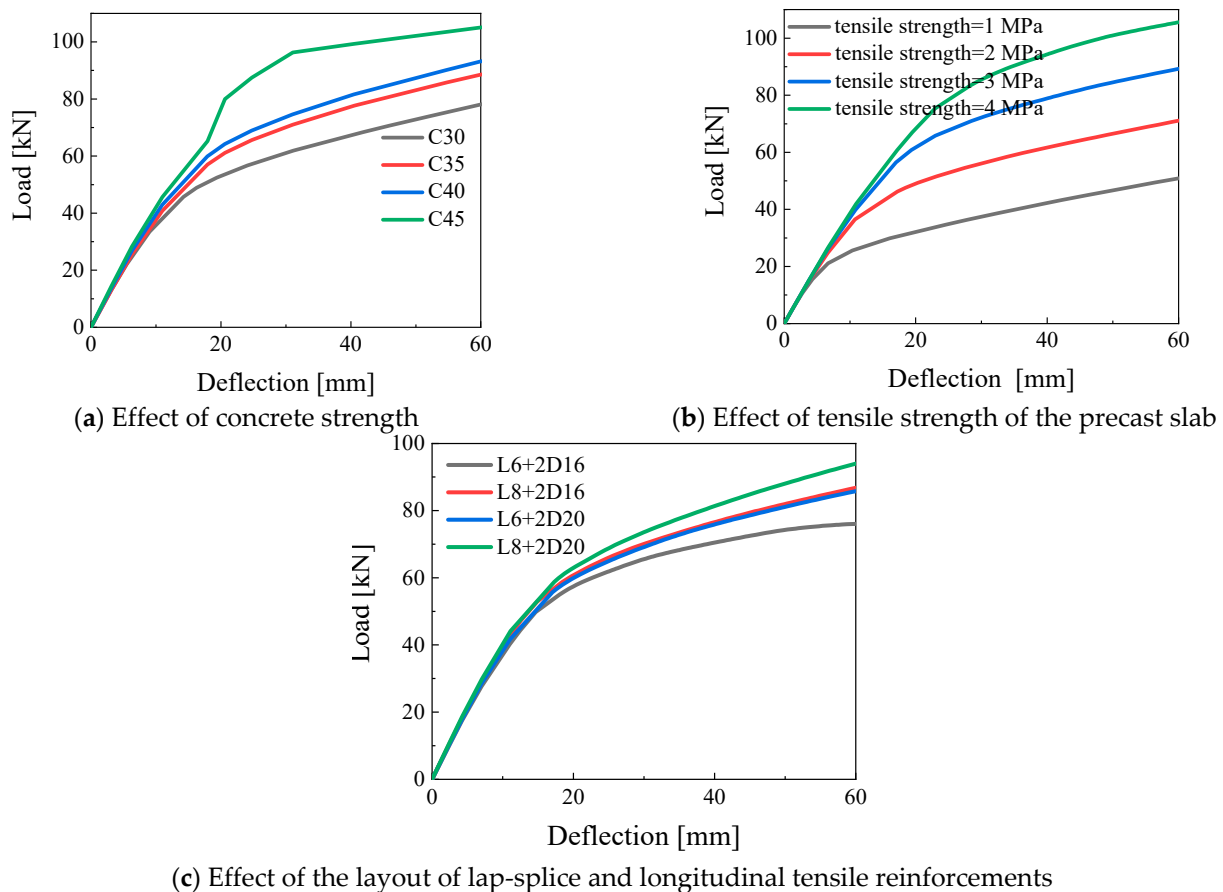
Figure 12. Comparisons of the load-midspan deflection.

To understand the flexural behavior of the proposed composite system, parametric FE analysis of PB-F-1-24-L was further conducted, as listed in Table 3, including the influences of concrete compressive strengths, bottom precast ribbed slab tensile strengths, and diameters of longitudinal tensile reinforcements at the joints and the lap-splice steel rebars. Figure 13a–c shows the load-midspan deflection curves affected by various parameters. Figure 13a indicates that, as the compressive strength increased from 30 MPa to 45 MPa, the ultimate strength increased by 20%. The approximate elastic stiffness and increasing post-cracking stiffness were observed with varying concrete compressive strengths. This was because increasing the concrete compressive strength positively decreased the midspan deflection and the cracking propagation under the same load level in the FE model. Figure 13b shows that, as the tensile strength increased from 1 MPa to 4 MPa, the ultimate loads increased by 87%. This was due to the fact that larger tensile strength delayed the crack propagation and increased the effective sectional stiffness, thereby leading to a higher ultimate load.

Additionally, the ultimate load increased with an increasing diameter of longitudinal and lap-splice steel reinforcements in the joints. When the diameter of longitudinal reinforcements increased from 16 to 20 mm, and the diameter of the lap-splice steel reinforcements increased from 6 to 8 mm, the failure load increased by 24% (see Figure 13c). The cracking loads and post-cracking stiffness also increased correspondingly. In contrast, the tensile strength of bottom precast slabs had a more significant influence on the ultimate loads of the composite slabs than the influences of the concrete compressive strength and joint connection strengths. It indicates that the tensile strength of precast slabs should be designed carefully to improve the ultimate bearing capacity of such composite slabs.

Table 3. Main parameters for the FE analysis.

Group	Parameters	Values
G-C-30	Concrete compressive strength f_c (MPa)	$f_c = 30$
G-C-35		$f_c = 35$
G-C-40		$f_c = 40$
G-C-45		$f_c = 45$
G-T-1	Precast ribbed slab tensile strengths f_t (MPa)	$f_t = 1$
G-T-2		$f_t = 2$
G-T-3		$f_t = 3$
G-T-4		$f_t = 4$
G-L6 + 2D16	Diameter of lap-splice steel rebars (L) and tensile steel reinforcements (D) (mm)	L6 + 2D16
G-L6 + 2D20		L6 + 2D20
G-L8 + 2D16		L8 + 2D16
G-L8 + 2D20		L8 + 2D20

**Figure 13.** Load-midspan deflection of PB-F-1-24-L affected by various parameters.

6. Conclusions

This study experimentally studied the flexural performances of precast composite floor systems with novel wet joints and steel sleeves. The influences of joint amounts, steel sleeve directions, casting methods, and shear span-to-depth ratio were considered. Based on the results of this study, the following conclusions can be drawn:

- (1) The precast composite slabs with steel sleeve connections in the joints could provide an ultimate bearing capacity comparable to the cast in situ concrete slabs. The cracks at the cast in situ and precast concrete interface and slip along the longitudinal steel reinforcements led to a smaller cracking load and larger midspan deflection.

- (2) The 2450 mm length composite slabs failed in flexural shear, while the flexural failure occurred for 4750 mm length composite slabs, characterized by the maximum crack width. Relative to the cast in situ concrete slabs, the precast composite slab had a relatively lower flexural capacity and stiffness due to interfacial splitting cracks.
- (3) No strain difference in the steel sleeves and longitudinal steel reinforcements was observed, and no failure occurring at the wet joints indicated that the proposed sleeve connection ensured reliable load transfer. The sleeve perpendicular to the moment had a minor influence on the interfacial cracking.
- (4) The tested ultimate moment was about 1.9 times the obtained design values calculated by the Chinese code. FE results indicated the tensile strength in the bottom precast slabs had a more significant influence on the ultimate bearing capacity than the influences of concrete compressive strength and wet joint strength when the connection strength was ensured.

Author Contributions: Conceptualization, W.Z. and Y.F.; Methodology, W.Z.; Software, X.Z.; Validation, L.G.; Formal analysis, W.Z.; Investigation, Y.F. and X.Z.; Data curation, Y.F.; Writing—original draft, X.Z. and L.R.; Writing—review & editing, M.X.; Visualization, L.R.; Supervision, M.X. and L.G.; Project administration, L.R.; Funding acquisition, M.X. and L.G. All authors have read and agreed to the published version of the manuscript.

Funding: This research was funded by Basic Science (Natural Science) Research Project of Higher Education Institutions in Jiangsu Province, 23KJA560006 and Project of Industry-University-Research Collaboration, BY20230056.

Data Availability Statement: The XLSX data used to support the findings of this study may be accessed by emailing to the corresponding author. The available time will be six months after the publication since there are still some researches and articles for submission based on this manuscript and the original data.

Acknowledgments: The support of Basic Science (Natural Science) Research Project of Higher Education Institutions in Jiangsu Province is gratefully acknowledged.

Conflicts of Interest: Author Xiangqiang Zeng was employed by the company Shandong Shijia Yuanda Technology Development Co., Ltd. The remaining authors declare that the research was conducted in the absence of any commercial or financial relationships that could be construed as a potential conflict of interest.

References

1. Pecce, M.R.; Ceroni, F.; Maddaloni, G. In-plane deformability of RC floors: Assessment of the main parameters and influence on dynamic behaviour. *Bull. Earthq. Eng.* **2019**, *17*, 297–311. [[CrossRef](#)]
2. Ahmed, I.M.; Tsavdaridis, K.D. The evolution of composite flooring systems: Applications, testing, modelling and eurocode design approaches. *J. Constr. Steel Res.* **2019**, *155*, 286–300. [[CrossRef](#)]
3. Bai, L.; Li, Y.; Hou, C.; Zhou, T.; Cao, M. Longitudinal shear behaviour of composite slabs with profiled steel sheeting and ECC. *Eng. Struct.* **2020**, *205*, 110085. [[CrossRef](#)]
4. Cao, X.; Li, X.; Zhu, Y.; Zhang, Z. A comparative study of environmental performance between prefabricated and traditional residential buildings in China. *J. Clean. Prod.* **2015**, *109*, 131–143. [[CrossRef](#)]
5. Hou, H.; Liu, X.; Qu, B.; Ma, T.; Liu, H.; Feng, M.; Zhang, B. Experimental evaluation of flexural behavior of composite beams with cast-in-place concrete slabs on precast prestressed concrete decks. *Eng. Struct.* **2016**, *126*, 405–416. [[CrossRef](#)]
6. Owolabi, D.; Loss, C. Experimental and numerical study on the bending response of a prefabricated composite CLT-steel floor module. *Eng. Struct.* **2022**, *260*, 114278. [[CrossRef](#)]
7. Wang, H.; Liu, X.; Yue, Q.; Zheng, M. Shear resistance of a novel wet connection for prefabricated composite beams under shear-bending coupling loading. *J. Build. Eng.* **2022**, *45*, 103636. [[CrossRef](#)]
8. Elamary, A.; Ahmed, M.M.; Mohmoud, A.M. Flexural behaviour and capacity of reinforced concrete–steel composite beams with corrugated web and top steel flange. *Eng. Struct.* **2017**, *135*, 136–148. [[CrossRef](#)]
9. Fahmy, M.F.M.; Sayed, A.H.; Farghal, O.A.; Ahmed, A.-E.M. Flexural Behavior of New Hybrid Profiled Steel-FRP T-Beams Filled with Concrete: Development and Validation. *J. Compos. Constr.* **2020**, *24*, 04020005. [[CrossRef](#)]
10. Ibrahim, I.S.; Elliott, K.S.; Abdullah, R.; Kueh, A.B.H.; Sarbini, N.N. Experimental study on the shear behaviour of precast concrete hollow core slabs with concrete topping. *Eng. Struct.* **2016**, *125*, 80–90. [[CrossRef](#)]

11. Lam, S.S.E.; Wong, V.; Lee, R.S.M. Bonding assessment of semi-precast slabs subjected to flexural load and differential shrinkage. *Eng. Struct.* **2019**, *187*, 25–33. [[CrossRef](#)]
12. Machado, W.G.; da Silva, A.R.; das Neves, F. de A. Dynamic analysis of composite beam and floors with deformable connection using plate, bar and interface elements. *Eng. Struct.* **2019**, *184*, 247–256. [[CrossRef](#)]
13. Baran, E. Effects of cast-in-place concrete topping on flexural response of precast concrete hollow-core slabs. *Eng. Struct.* **2015**, *98*, 109–117. [[CrossRef](#)]
14. Adawi, A.; Youssef, M.A.; Meshaly, M.E. Experimental investigation of the composite action between hollowcore slabs with machine-cast finish and concrete topping. *Eng. Struct.* **2015**, *91*, 1–15. [[CrossRef](#)]
15. Yardim, Y.; Waleed, A.M.T.; Jaafar, M.S.; Laseima, S. AAC-concrete light weight precast composite floor slab. *Constr. Build. Mater.* **2013**, *40*, 405–410. [[CrossRef](#)]
16. Pang, R.; Zhang, Y.; Dang, L.; Zhang, L.; Liang, S. Experimental and numerical investigation on the vertical bearing behavior of discrete connected new-type precast reinforced concrete floor system. *Adv. Struct. Eng.* **2020**, *23*, 2276–2291. [[CrossRef](#)]
17. Li, S.; Chen, W.; Zhang, Y. Flexural behavior of precast, prestressed, lightweight aggregate concrete-conventional concrete composite beams. *Constr. Build. Mater.* **2021**, *274*, 121926. [[CrossRef](#)]
18. Qi, J.; Yang, H.-C. Improvement of a Truss-Reinforced, Half-Concrete Slab Floor System for Construction Sustainability. *Sustainability* **2021**, *13*, 3731. [[CrossRef](#)]
19. Ghayeb, H.H.; Razak, H.A.; Ramli Sulong, N.H. Performance of dowel beam-to-column connections for precast concrete systems under seismic loads: A review. *Constr. Build. Mater.* **2020**, *237*, 117582. [[CrossRef](#)]
20. Chen, Y.; Shi, H.-R.; Wang, C.-L.; Wu, J.; Liao, Z.-Q. Flexural mechanism and design method of novel precast concrete slabs with crossed bent-up rebar. *J. Build. Eng.* **2022**, *50*, 104216. [[CrossRef](#)]
21. Huang, Y.; Yang, J.; Zhong, C. Flexural performance of assembly integral floor structure voided with steel mesh boxes. *J. Build. Eng.* **2022**, *54*, 104693. [[CrossRef](#)]
22. Deng, B.-Y.; Tan, D.; Li, L.-Z.; Zhang, Z.; Cai, Z.-W.; Yu, K.-Q. Flexural behavior of precast ultra-lightweight ECC-concrete composite slab with lattice girders. *Eng. Struct.* **2023**, *279*, 115553. [[CrossRef](#)]
23. Zeng, X.; Feng, Y.; Ruan, S.; Xu, M.; Gong, L. Experimental and Numerical Study on Flexural Behavior of a Full-Scale Assembled Integral Two-Way Multi-Ribbed Composite Floor System. *Buildings* **2023**, *13*, 2517. [[CrossRef](#)]
24. GB 50010-2010; Design Code for Concrete Structure. China Architecture & Building Press: Beijing, China, 2017.
25. GB/T 50152-2012; Standard for Test Method of Concrete Structures. China Architecture & Building Press: Beijing, China, 2012.
26. ABAQUS. *Documentation 6.14*; Dassault System: Vélizy-Villacoublay, France, 2013.
27. Figiel, Ł.; Kamiński, M. Numerical Probabilistic Approach to Sensitivity Analysis in a Fatigue Delamination Problem of a Two Layer Composite. *Appl. Math. Comput.* **2009**, *209*, 75–90. [[CrossRef](#)]

Disclaimer/Publisher’s Note: The statements, opinions and data contained in all publications are solely those of the individual author(s) and contributor(s) and not of MDPI and/or the editor(s). MDPI and/or the editor(s) disclaim responsibility for any injury to people or property resulting from any ideas, methods, instructions or products referred to in the content.